Reversible Photo-induced Doping in WSe2 Field Effect Transistors

Journal:	*Nanoscale*
Manuscript ID	NR-ART-12-2018-009929.R1
Article Type:	Paper
Date Submitted by the Author:	25-Feb-2019
Complete List of Authors:	Luo, Xuyi; Vanderbilt University, Electrical Engineering and Computer Science Andrews, Kraig; Wayne State University Wang, Tianjiao; Vanderbilt University, Electrical Engineering and Computer Science Bowman, Arthur; Wayne State University Zhou, Zhixian; Wayne State University Xu, Yaqiong; Vanderbilt University, Electrical Engineering and Computer Science

SCHOLARONE™
Manuscripts

Reversible Photo-induced Doping in WSe$_2$ Field Effect Transistors

Xuyi Luo[1], Kraig Andrews[2], Tianjiao Wang[1], Arthur Bowman[2], Zhixian Zhou[2],

and Ya-Qiong Xu[,1,3]*

[1]Department of Electrical Engineering and Computer Science, Vanderbilt University, Nashville, TN 37235, USA

[2]Department of Physics and Astronomy, Wayne State University, Detroit, MI 48201, USA

[3]Department of Physics and Astronomy, Vanderbilt University, Nashville, TN 37235, USA

*Correspondence to: yaqiong.xu@vanderbilt.edu

Abstract

We report a reversible photo-induced doping effect in two-dimensional (2D) tungsten diselenide (WSe_2) field effect transistors on hexagonal boron nitride (h-BN) substrates under low-intensity visible light illumination (~ 10 nW/μm^2). Our experimental results have shown that this reversible doping process is mainly attributed to two types of defects in h-BN substrates. Moreover, the photo-doped WSe_2 transistors can be stable for more than one week in a dark environment and maintain the high on/off ratio (10^8) and carrier mobility, since there are no additional impurities involved during the photo-induced doping process to increase the columbic scattering in the conducting channel. These fundamental studies not only provide an accessible strategy to control the charge doping level and then to achieve a writing/erasing process in 2D transistors, but also shed light on the defect states and interfaces in 2D materials.

Keywords: WSe_2, photoresponse, TMDs, h-BN defects, doping

Introduction

Graphene has aroused great interest during the last decade owing to their extraordinary properties for both fundamental physics and promising optoelectronic applications.[1-7] Though graphene has very high mobility, there is a key bottleneck for graphene-based transistors that its on/off ratio is very small due to the gapless nature of graphene.[1] Superior to graphene, transition metal dichalcogenides (TMDs) have opened up new opportunities for two-dimensional (2D) electronics and optoelectronics such as transistors, memories, photodetectors, and integrated circuits, because they have tunable band gaps with selectable electronic properties ranging from metallic to semiconducting.[8-17] Particularly for semiconducting TMDs such as MoX_2 and WX_2 compounds (X is a chalcogen), their relatively large band gaps in the range of 1-2 eV lead to high on/off ratios in TMD-based transistors. Moreover，the advantages of the immunity of short-channel effect and ultralow power dissipation make TMDs ideal channel materials for extending the scaling limit for future transistor miniaturization.[18, 19]

The modulation of charge carriers in semiconducting materials is the foundation to implement various functional electronic and optoelectronic devices.[20, 21] As the thickness of semiconducting materials decreases to the atomic scale, the efficient carrier modulation becomes more critical but confronts numerous unprecedented challenges. Traditional doping technologies, such as atomic substitutions[22, 23] and plasma treatment,[24] may introduce abundant defects in intrinsic lattice structures, compromising the carrier mobility of TMDs. Other defect-free doping approaches reported recently are based on charge transfer between TMDs and gases,[25] ions,[26] nanoparticles,[27] etc. These methods, however, usually suffer from long-term stability issue[28] and involve solution-based

processes, which are hardly compatible with standard CMOS processes. Recently, photo-induced doping has been demonstrated in graphene transistors.[29, 30] Although the reported photo-induced doping process was rapid and defect-free, the relatively high intensity of light ($\sim$ 1 - 600 $\mu W/\mu m^2$) with the excitation light wavelength below 500 nm and the gapless nature of graphene limit the digital application of photo-doped graphene transistors.[29, 30]

Here we report the photo-induced doping effect in tungsten diselenide (WSe_2) field effect transistors (FET) on h-BN substrates under 640 nm illumination with a light intensity of 10 $nW/\mu m^2$. The charge doping level of WSe_2 can be controllably and reversibly modified through optical processes. More importantly, this photo-induced doping process does not compromise the high on/off ratio (10^8) and carrier mobility of WSe_2 since no dopant is introduced in the conducting channel. Our experimental results suggest that the photo-induced doping effect primarily comes from two types of defects in h-BN flakes. A strong interaction between incident photons and the defects of h-BN substrates alters their local electrostatic environments, leading to a shift of the threshold voltage of WSe_2 FETs. In addition, these fundamental studies offer a way to explore the defect states in h-BN substrates and barriers at WSe_2/h-BN interfaces, which are directly associated with the photo-induced doping effect in WSe_2 channels.

Results and discussion

Figure 1a shows the schematic diagram of a WSe_2 FET composed of degenerately p-doped WSe_2 ($Nb_{0.005}W_{0.995}Se_2$) 2D drain/source electrodes in contact with an undoped 2D WSe_2 channel. To provide a smooth substrate and enhance the mobility of WSe_2, a h-

BN flake was placed between the undoped WSe_2 channel and the highly-doped Si substrate covered with a 280-nm-thick SiO_2 layer.[31] Both WSe_2 and h-BN flakes were obtained by mechanical exfoliation from their bulk crystals. The degenerately p-doped WSe_2 flakes were artificially stacked on top of the undoped WSe_2 flake via a dry transfer method to achieve low-resistance ohmic contacts.[32] Metal electrodes were then fabricated atop the degenerately-doped source and drain contacts by standard electron beam lithography (EBL) and subsequent deposition of 5 nm of Ti covered by 50 nm of Au. Figure 1b presents the optical image of a typical device with an 3.1 nm thick (~ 5 layers) WSe_2 channel as identified by atomic force microscopy (AFM). Degenerately p-doped WSe_2 contacts, undoped WSe_2 channel and h-BN flakes are outlined by colored dashed lines. Back-gate biases were applied to the WSe_2 channel via the highly-doped Si substrate through a dielectric stack consisting of a 30 nm thick h-BN flake and 280 nm thick SiO_2. The electrical properties of the device were characterized under high vacuum (~10^{-6} Torr) at 77 K in a Janis ST-500 cryostat. As shown in Figure 1c, the transport characteristics of the WSe_2 device displays a p-type behavior with a high on/off ratio of 10^8 and a hole mobility of 123 $cm^2V^{-1}s^{-1}$, which are consistent with our previous reports.[12, 32] The hole mobility is calculated from the linear region of the transfer curve by using the expression $\mu = (1/C_{bg}) \times (L/W) \times (d\sigma/dVg)$, where L, W, and σ represent the length, width and conductance of the channel, and C_{bg} is the back-gate capacitance of the h-BN/SiO_2 dielectric. Figure 1d shows linear output characteristics of the WSe_2 FET when various back-gate voltages were applied, indicating ohmic behavior of the device.

We have also found the charge doping level of WSe_2 FETs on h-BN substrates can be modulated by light illumination. In our experiments, the device was exposed to

light with the intensity of ~ 10 nW/μm² at a fixed back-gate voltage (V_g^{light}) and then transport measurements were performed after the light turned off. The illumination time was chosen to be so long that the transport curve became stable or the photo-induced doping process was saturated. To maintain the same initial state of the WSe₂ FET (orange line in Figure 2a), the device was exposed to an X-Cite 120Q light source at $V_g^{light} = 0\ V$ for 5 min to erase the photo-induced doping effect before each test. Figure 2a shows the transport measurements of the photo-doped WSe₂ FET when V_g^{light} was stepped from -10 V to -30 V in -10 V intervals under 460 nm illumination. The photo-induced doping leads to a shift of the threshold voltage by the V_g^{light} set point, suggesting an n-type doping effect. More importantly, the gate-dependent characteristics of the photo-doped WSe₂ FET is similar to that of the undoped one, indicating that the photo-induced modulation is a homogeneous doping process throughout the entire device with a negligible effect on the high on/off ratio and carrier mobility of WSe₂. Moreover, we investigated the photo-induced doping effect in the WSe₂ FET under $V_g^{light} = -30\ V$ with different excitation wavelengths. As shown in Figure 2b, there is no significant difference in transport characteristics between the 640 nm-doped WSe₂ FET and the 460 nm-doped one. This is different from the previous study, where only blue or violet light sources can efficiently modulate the charge doping level of graphene flakes on h-BN substrates.[30] Interestingly, when the WSe₂ FET was exposed to 820 nm illumination, a negligible doping-effect was observed.

To further investigate the relationship between the doping effect and the light wavelength or photon energy, we explored the charge doping efficiency for various photon energies. Here the source-drain current (I_{ds}) was recorded when the WSe₂ FET

was under illumination (10 nW/μm²) with a 50-mV source-drain bias (V_{ds}) and a gate

voltage of $V_g^{light} = -50\ V$. During the photo-induced doping process, I_{ds} decreased. The

charge doping time (*t*) is defined as the time required for I_{ds} decreasing from 90% to

10%; and the charge doping efficiency is defined as *1/t*. As shown in Figure 2c, the

charge doping effect is negligible when the photon energy is less than 1.9 eV, while the

charge doping effect increases drastically when the photon energy exceeds 2.2 eV. Since

h-BN is an insulator with the bandgap of 6.0 eV,[33] the visible light cannot excite the

electrons from its valance band to conduction band. Moreover, photo-induced hot carriers

may have limited effect on the WSe₂ FETs on h-BN substrates since their relaxation in

graphene on h-BN substrates is much faster than that directly on SiO₂ substrates.[34]

Therefore, the photo-induced doping effect is likely related to the defect states in h-BN

substrates. For photon energy between 1.9 eV and 2.2 eV, the charge doping effect may

result from the N_BV_N defect (a nitrogen atom at a boron site neighboring a vacancy) in

the bulk of h-BN since an internal transition of 1.9 eV has been demonstrated for the

N_BV_N defect states in h-BN.[35] The strong increase in the charge doping efficiency for the

photon energy above 2.2 eV is likely related to the direct transition from both the N_BV_N

and nitrogen vacancy (V_N) in crystalline h-BN. The V_N defect state has been predicted at

2.8 eV in a theoretical study.[33] In fact, similar results have been observed in graphene/h-

BN heterojunctions, where the electrons in the V_N defect state of h-BN can be excited by

the light illumination with a wavelength below 500 nm.[30]

Figure 3a shows the band diagram of WSe₂/h-BN heterostructures under

equilibrium conditions and the red dashed line denotes the Fermi level of WSe₂. Under

460 nm illumination with $V_g^{light} < 0$ V (Figure 3b), the electrons in the V_N (blue dashed

line) and N_BV_N (blue dotted line) defect states of h-BN can obtain enough energy to be excited to the conduction band of h-BN and then drift to the conduction band of WSe_2 through the electric field induced by the negative gate voltage, leading to the n-type doping in WSe_2. Positively-charged defects in h-BN flakes can also produce an electric field that will eventually balance the gate-voltage-induced electric field. Under 640 nm illumination with $V_g^{light} < 0$ V (Figure 3c), the electrons in the V_N defect state cannot get enough energy to directly jump into the conduction band of h-BN; but the photon can excite these electrons from the ground state to the excited state (1.95 eV above its ground state) of the N_BV_N defect in h-BN.[35] After that, the excited electrons can absorb photons and jump into the conduction band of h-BN. Here, the excited state of the N_BV_N defect acts as a ladder to boost the photo-doping process for the photons with energies ranging from 1.9 eV to 2.2 eV. The electrons then flow to the conduction band of WSe_2 under the gate-voltage-induced electric field. The charge transfer continues until the applied electric field gets fully screened by the positively-charged defects in h-BN flakes. This ladder-assisted doping process (640 nm) is not as efficient as the doping process induced by 460 nm illumination since the 460 nm light can directly excite the electrons from both V_N and N_BV_N defect states to the conduction band in h-BN.

Moreover, when the gate voltage set back to 0 V, the electrons in the WSe_2 channel cannot move back to the h-BN flake due to the existence of the barrier at the WSe_2/h-BN interface (Figure 3d). As a result, the WSe_2 channel maintains the n-doped and the h-BN flake remains positively charged. Without efficient discharge channels, the photo-doped WSe_2 FET is stable for more than a week under high vacuum condition with a dark environment (Figure S1). Interestingly, the photo-doped device can be easily

restored by 460 nm illumination. Figure 4a shows the transport measurements of the WSe$_2$ FET before and after photo-induced doping. State I is referred to the device prior to the light exposure (black). State II represents the device that is completely doped under 460 nm illumination with a gate voltage of $V_g^{light} = -30\ V$ (red). We could restore the device from State II to State I by using 460 nm light with the power intensity of $\sim$ 0.3 µW/ µm^2 at $V_g = 0\ V$. Figure 4b displays the restoring effect versus time. ΔV_{th} denotes the threshold voltage (V_{th}) shift of the device compared to that of State I. During the 460 nm illumination, $|\Delta V_{th}|$ decreases and the transport curve gradually shifts to that of the device before photo-induced doping (State I). This suggests that the high energy photons could excite the electrons in the WSe$_2$ channel, make them overcome the barrier at the WSe$_2$/h-BN interface, recombine with positively-charged defects in the h-BN substrate, and restore the photo-doped WSe$_2$ FET to State I. More interestingly, the restoring efficiency drops after the first minute, since more and more fixed positively-charged defects in h-BN are neutralized by the photo-excited electrons from the WSe$_2$ channel, leading to a reduced concentration of positively-charged defects and thus a low restoring efficiency. To compare the photo-induced restoring effect with different illumination wavelengths, we also exposed the photo-doped device (State II) to 500 nm and 540 nm laser beams (Figure 4c), respectively, with the power intensity of $\sim$ 0.3 µW/ µm^2 at $V_g = 0\ V$. For 2.3 eV photons (540 nm), the restoring effect is negligible for the photo-doped WSe$_2$ FET, indicating these photons cannot provide enough energy to make the electrons in the WSe$_2$ channel to overcome the barrier at the WSe$_2$/h-BN interface. When the photon energy is above 2.3 eV (e.g. 500 nm), some electrons in the WSe$_2$ channel can go through the interface barrier, flow into the h-BN substrate, and then neutralize their

positively-charged defects. These fundamental studies not only offer a way to study the defect states of h-BN flakes and the barriers at WSe_2/h-BN interfaces, but also provide a strategy to precisely and reversibly control the charge doping level in WSe_2 FETs.

Conclusion

In summary, an efficient and controllable photo-induced doping process in WSe_2 FETs on h-BN substrates has been demonstrated to preserve the high on/off ratio and carrier mobility of WSe_2 FETs, allowing for repeatable writing and erasing of the doping features at both room temperature and low temperature (Figure S2). Wavelength-dependent measurements suggest that the photo-induced doping process is mainly attributed to the V_N and N_BV_N defects in h-BN substrates and the restoring process is likely related to the barriers at WSe_2/h-BN interfaces. These fundamental studies not only shed light on the knowledge about the defect states and interfaces of 2D materials, but also provide a novel and simple technique to control the charge doping levels in 2D materials, enabling many possibilities toward fantastic photo-controllable electronic devices, such as the optical trigger non-voltaic memory.

Methods

Device fabrication

10 - 40 nm thick h-BN flakes were produced from h-BN bulks by a mechanical cleavage method and subsequently transferred onto highly-doped silicon substrate covered with a 280 nm-thick thermal oxide layer. Atomically thin flakes of undoped WSe_2 were exfoliated from bulk crystals onto a PDMS stamp, subsequently transferred onto selected thin h-BN flakes on the SiO_2/Si substrate via a precision transfer stage. To make 2D/2D

contacts, degenerately-doped WSe_2 flakes are exfoliated onto SiO_2/Si substrates, patterned into drain/source electrodes by EBL and SF6 dry etching, and then transferred to the two exposed ends of the undoped WSe_2 channel as drain/source contacts using a pick-up method. To improve the interface quality between the h-BN and WSe_2 channel as well as between the doped WSe_2 drain/source contacts and WSe_2 channel, a mild annealing step was carried out after each transfer step at 250 ℃ for 30 minutes in a vacuum chamber purged by 10% H_2 and 90% Ar. The dimensions (e.g. the sample thickness) and the surface quality (e.g. the cleanness and smoothness) of the h-BN substrate and WSe_2 channel were characterized by Park Systems AFM in the non-contact mode after each annealing step (Figure S3). Metal electrodes, consisting of 5 nm of Ti and 50 nm of Au, were fabricated to electrically wire up the degenerately-doped WSe_2 drain/source electrodes using standard EBL and electron beam deposition.

Electrical and optoelectronics characteristics

Electrical properties of the devices were measured by a Keithley 4200 semiconductor parameter analyzer in a lakeshore Cryogenic probe station. Optoelectronic measurements were performed in an Olympus microscope setup (BX51W). A linearly-polarized continuous wave laser beam (NKT Photonics SuperK Supercontinuum Laser) was expanded and focused by a 40X objective (N.A. = 0.6) into a diffraction-limited laser spot (~1 μm in diameter) on devices. The position of the laser beam was changed by a nanometer-resolution scanning mirror and its polarization direction was changed by a half-wave plate followed by a polarizer. All experiments were performed at 77 K under high vacuum (1×10^{-6} Torr).
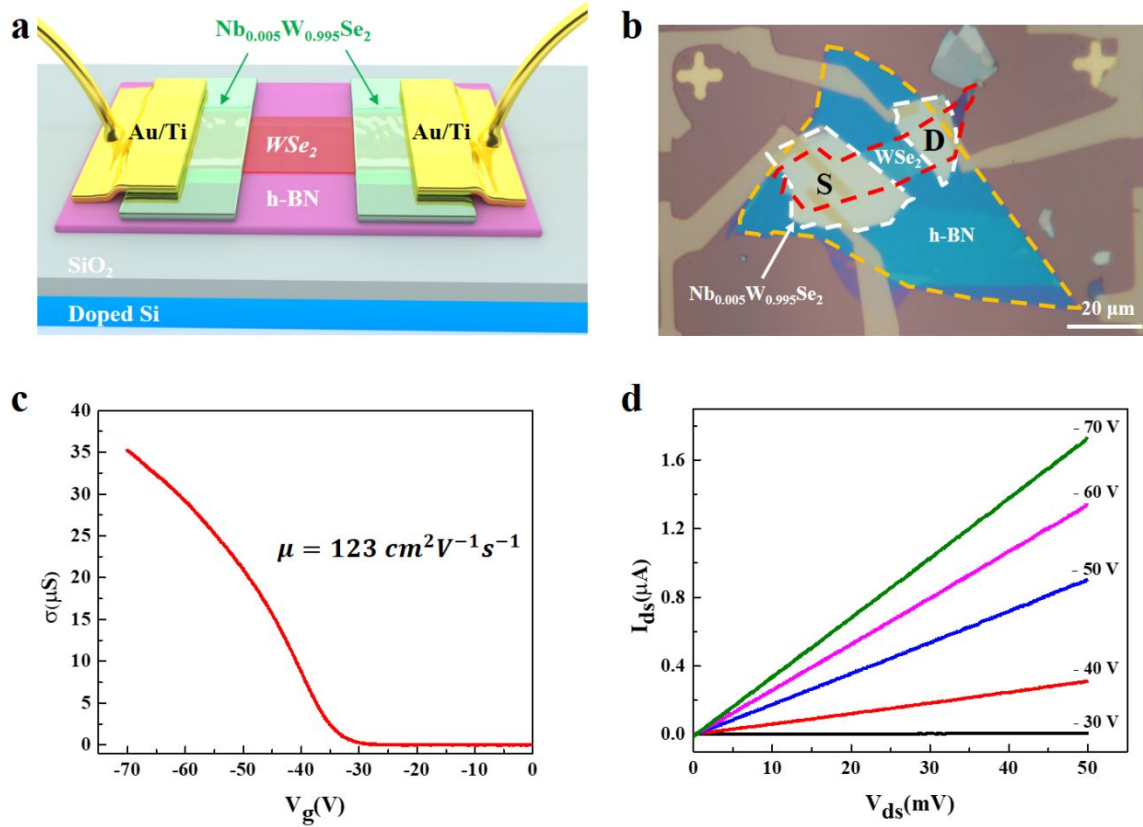
**Conflicts of interest**

13

There are no conflicts to declare.

Acknowledgments

Figures

Figure 1. Configuration and characteristics of a WSe$_2$ FET with 2D/2D contacts. (a) Perspective side view of a WSe$_2$ FET with degenerately p-doped WSe$_2$ (Nb$_{0.005}$W$_{0.995}$Se$_2$) contacts. (b) Optical image of the device. The gold dashed line outlines the h-BN thin film. The white and red dashed lines represent the outlines of the Nb-doped WSe$_2$ contacts and undoped WSe$_2$ channel, respectively. (c) Modulation of the source-drain conductance by the back-gate voltage (V$_g$) at 77 K. (d) Linearity of the I$_{ds}$−V$_{ds}$ characteristics indicating ohmic behaviors for a wide range of back-gate voltages.
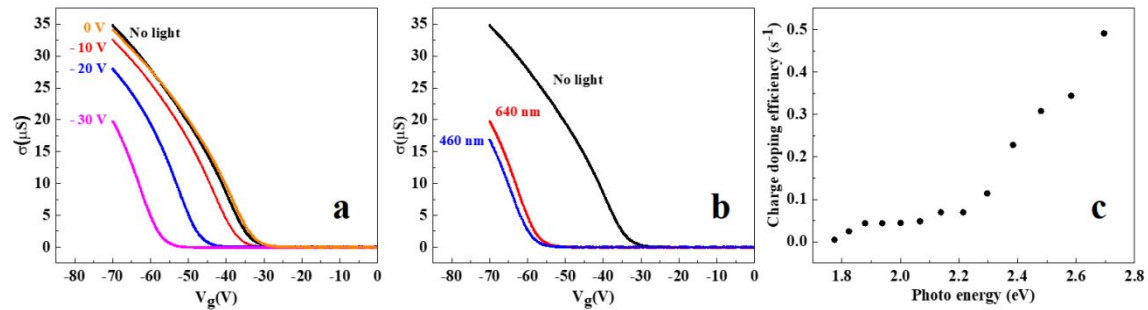
Figure 2. Experimental observation of the photo-induced doping in the WSe$_2$ FET.

(a) Transport curves after 460 nm (~ 0.01 µW/µm^2) illumination with different back-gate voltages: $V_g^{light} = 0V, -10V, -20V, and -30V,$ respectively. (b) Transport curves after 460 nm and 640 nm illumination with $V_g^{light} = -30\ V$. (c) Photo-induced doping efficiency as a function of photon energy with $V_g^{light} = -50\ V$.
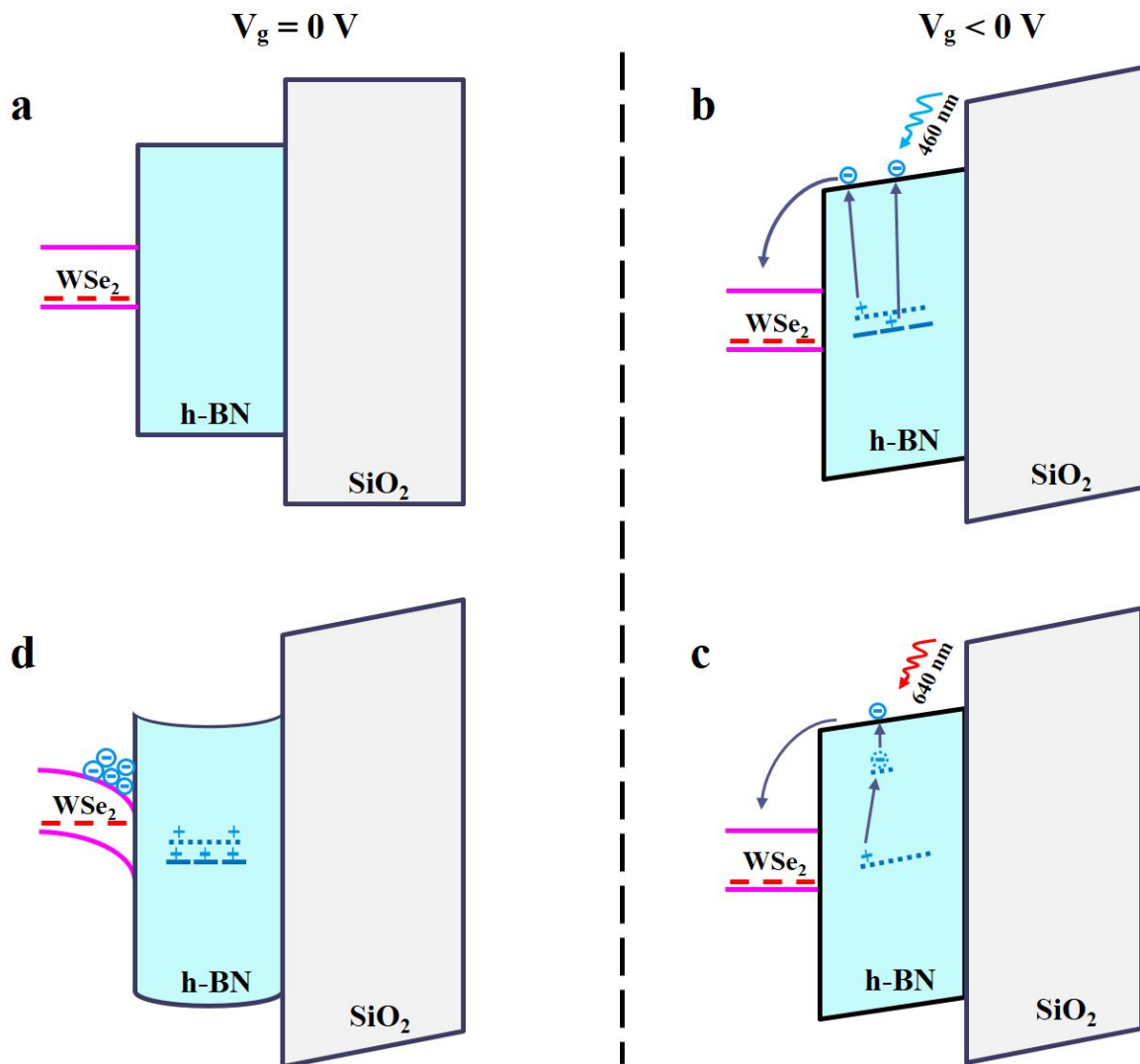
Figure 3. Photo-induced doping mechanisms for WSe$_2$ FETs on h-BN substrates. The red dash lines correspond to the Fermi level of the undoped WSe$_2$ channel. Blue dashed and dotted lines represent V_N and N_BV_N defect states in h-BN substrates, respectively. (a) The band diagram of the WSe$_2$ FET under equilibrium conditions (V_g = 0 V). The band diagrams of the WSe$_2$ FET with $V_g^{light} < 0$ V under (b) 460 nm and (c) 640 nm illumination, respectively. (d) The band diagram of the photo-doped WSe$_2$ FET after the doping process is completed with V_g = 0 V.
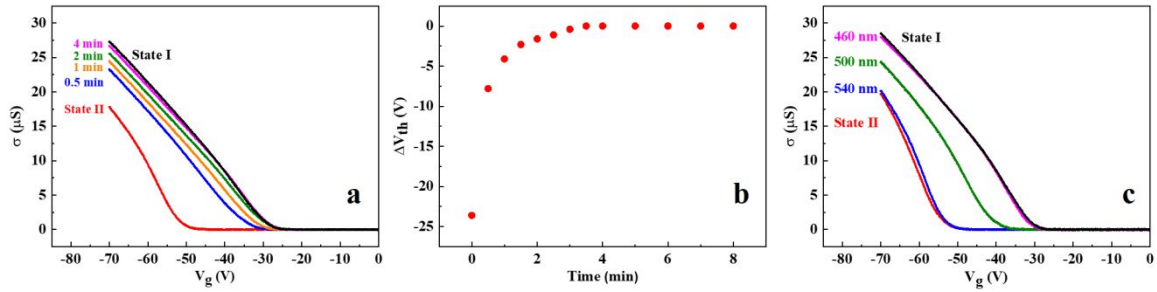
Figure 4. The comparison of the restoring process in WSe₂/h-BN heterostructures under illumination with different wavelengths. (a) State I and State II represent the response of the device before and after 460 nm illumination with $V_g^{light} = -30\,V$, respectively. (b) The restoring process under 460 nm illumination with $V_g^{light} = 0\,V$. ΔV_{th} denotes the threshold voltage (V_{th}) shift of the device compared to that of State I. (c) During the restoring process, the device is tested with a back-gate voltage of $V_g^{light} = 0V$ under 540 nm, 500 nm and 460 nm illumination, respectively.

References

1.   K. S. Novoselov, A. K. Geim, S. V. Morozov, D. Jiang, Y. Zhang, S. V. Dubonos, I. V. Grigorieva and A. A. Firsov, *Science*, 2004, **306**, 666.
2.   K. S. Novoselov, A. K. Geim, S. V. Morozov, D. Jiang, M. I. Katsnelson, I. V. Grigorieva, S. V. Dubonos and A. A. Firsov, *Nature*, 2005, **438**, 197-200.
3.   T. J. Wang and Y. Q. Xu, *Electronics*, 2016, **5**, 93.
4.   F. Bonaccorso, Z. Sun, T. Hasan and A. C. Ferrari, *Nat Photonics*, 2010, **4**, 611-622.
5.   R. Wang, T. Hong and Y. Q. Xu, *Acs Appl Mater Inter*, 2015, **7**, 5233-5238.
6.   T. Hong, Y. Cao, D. Ying and Y.-Q. Xu, *Appl Phys Lett*, 2014, **104**, 223102.
7.   Q. Bao and K. P. Loh, *Acs Nano*, 2012, **6**, 3677-3694.
8.   B. Radisavljevic, A. Radenovic, J. Brivio, V. Giacometti and A. Kis, *Nature Nanotechnology*, 2011, **6**, 147-150.
9.   H. Wang, L. Yu, Y.-H. Lee, Y. Shi, A. Hsu, M. L. Chin, L.-J. Li, M. Dubey, J. Kong and T. Palacios, *Nano Letters*, 2012, **12**, 4674-4680.
10.   O. Lopez-Sanchez, D. Lembke, M. Kayci, A. Radenovic and A. Kis, *Nature Nanotechnology*, 2013, **8**, 497-501.
11.   R. Wang, T. J. Wang, T. Hong and Y. Q. Xu, *Nanotechnology*, 2018, **29**.
12.   T. Wang, K. Andrews, A. Bowman, T. Hong, M. Koehler, J. Yan, D. Mandrus, Z. Zhou and Y.-Q. Xu, *Nano Letters*, 2018, **18**, 2766-2771.
13.   K. F. Mak and J. Shan, *Nat Photon*, 2016, **10**, 216-226.
14.   T. Wang, S. Hu, B. Chamlagain, T. Hong, Z. Zhou, S. M. Weiss and Y.-Q. Xu, *Advanced Materials*, 2016, **28**, 7162-7166.
15.   W. J. Yu, Z. Li, H. Zhou, Y. Chen, Y. Wang, Y. Huang and X. Duan, *Nat Mater*, 2012, **12**, 246.
16.   T. S. Walmsley, B. Chamlagain, U. Rijal, T. Wang, Z. Zhou and Y.-Q. Xu, *Advanced Optical Materials*, 2018.
17.   H. Wang, L. L. Yu, Y. H. Lee, Y. M. Shi, A. Hsu, M. L. Chin, L. J. Li, M. Dubey, J. Kong and T. Palacios, *Nano Letters*, 2012, **12**, 4674-4680.
18.   H. Liu, A. T. Neal and P. D. Ye, *Acs Nano*, 2012, **6**, 8563-8569.
19.   S. B. Desai, S. R. Madhvapathy, A. B. Sachid, J. P. Llinas, Q. Wang, G. H. Ahn, G. Pitner, M. J. Kim, J. Bokor, C. Hu, H.-S. P. Wong and A. Javey, *Science*, 2016, **354**, 99-102.
20.   G. R. Bhimanapati, Z. Lin, V. Meunier, Y. Jung, J. Cha, S. Das, D. Xiao, Y. Son, M. S. Strano, V. R. Cooper, L. Liang, S. G. Louie, E. Ringe, W. Zhou, S. S. Kim, R. R. Naik, B. G. Sumpter, H. Terrones, F. Xia, Y. Wang, J. Zhu, D. Akinwande, N. Alem, J. A. Schuller, R. E. Schaak, M. Terrones and J. A. Robinson, *Acs Nano*, 2015, **9**, 11509-11539.
21.   R. Saran and R. J. Curry, *Nat Photonics*, 2016, **10**, 81-92.
22.   X. Duan, C. Wang, Z. Fan, G. Hao, L. Kou, U. Halim, H. Li, X. Wu, Y. Wang, J. Jiang, A. Pan, Y. Huang, R. Yu and X. Duan, *Nano Letters*, 2016, **16**, 264-269.
23.   E. H. Åhlgren, J. Kotakoski and A. V. Krasheninnikov, *Phys Rev B*, 2011, **83**, 115424.
24.   A. Nipane, D. Karmakar, N. Kaushik, S. Karande and S. Lodha, *Acs Nano*, 2016, **10**, 2128-2137.

25.	S. Tongay, J. Zhou, C. Ataca, J. Liu, J. S. Kang, T. S. Matthews, L. You, J. Li, J. C. Grossman and J. Wu, *Nano Letters*, 2013, **13**, 2831-2836.
26.	X. Liu, D. Qu, J. Ryu, F. Ahmed, Z. Yang, D. Lee and W. J. Yoo, *Advanced Materials*, 2016, **28**, 2345-2351.
27.	D. Sarkar, X. Xie, J. Kang, H. Zhang, W. Liu, J. Navarrete, M. Moskovits and K. Banerjee, *Nano Letters*, 2015, **15**, 2852-2862.
28.	H. Fang, M. Tosun, G. Seol, T. C. Chang, K. Takei, J. Guo and A. Javey, *Nano Letters*, 2013, **13**, 1991-1995.
29.	Y. D. Kim, M.-H. Bae, J.-T. Seo, Y. S. Kim, H. Kim, J. H. Lee, J. R. Ahn, S. W. Lee, S.-H. Chun and Y. D. Park, *Acs Nano*, 2013, **7**, 5850-5857.
30.	L. Ju, J. Velasco Jr, E. Huang, S. Kahn, C. Nosiglia, H.-Z. Tsai, W. Yang, T. Taniguchi, K. Watanabe, Y. Zhang, G. Zhang, M. Crommie, A. Zettl and F. Wang, *Nature Nanotechnology*, 2014, **9**, 348.
31.	C. R. Dean, A. F. Young, I. Meric, C. Lee, L. Wang, S. Sorgenfrei, K. Watanabe, T. Taniguchi, P. Kim, K. L. Shepard and J. Hone, *Nature Nanotechnology*, 2010, **5**, 722.
32.	H.-J. Chuang, B. Chamlagain, M. Koehler, M. M. Perera, J. Yan, D. Mandrus, D. Tománek and Z. Zhou, *Nano Letters*, 2016, **16**, 1896-1902.
33.	C. Attaccalite, M. Bockstedte, A. Marini, A. Rubio and L. Wirtz, *Phys Rev B*, 2011, **83**, 144115.
34.	D. Golla, A. Brasington, B. J. LeRoy and A. Sandhu, *APL Materials*, 2017, **5**, 056101.
35.	T. T. Tran, K. Bray, M. J. Ford, M. Toth and I. Aharonovich, *Nature nanotechnology*, 2016, **11**, 37.